Cell Biology

BMP9 and BMP10 coordinate liver cellular crosstalk to maintain liver health

Reviewed Preprint

Published from the original preprint after peer review and assessment by eLife.

About eLife's process

Reviewed preprint version 1
April 12, 2024 (this version)

Posted to preprint server
February 9, 2024

Sent for peer review
February 8, 2024

Dianyuan Zhao, Ziwei Huang, Xiaoyu Li, Huan Wang, Qingwei Hou, Yuyao Wang, Fang Yan, Wenting Yang, Di Liu, Shaoqiong Yi, Chunguang Han, Yanan Hao, Li Tang

State Key Laboratory of Medical Proteomics, Beijing Proteome Research Center, National Center for Protein Sciences (Beijing), Beijing Institute of Lifeomics, Beijing, 102206, P.R. China • Department of Immunology, School of Basic Medical Sciences, Anhui Medical University, Hefei, Anhui Province, 230032, P.R. China • School of Basic Medicine, Qingdao University, Qingdao, Shandong Province, 266071, P.R. China

Abstract

The liver is the largest solid organ in the body and is primarily composed of HCs, ECs, KCs, and HSCs, which spatially interact and cooperate with each other to maintain liver homeostasis. However, the complexity and molecular mechanisms underlying the crosstalk between these different cell types remain to be revealed. Here, we generated mice with conditional deletion of *Bmp9/10* in different liver cell types and demonstrated that HSCs were the major source of BMP9 and BMP10 in the liver. Using transgenic ALK1 (receptor for BMP9/10) reporter mice, we found that ALK1 is expressed on KCs and ECs other than HCs and HSCs. KCs from *Bmp9/10*$^{\text{HSC-KO}}$ (conditional deletion of *Bmp9/10* from HSCs) mice lost their signature gene expression, such as ID1/3, CLEC4F, VSIG4 and CLEC2, and were replaced by monocyte-derived macrophages. ECs from *Bmp9/10*$^{\text{HSC-KO}}$ mice also lost their identity and were transdifferentiated into continuous ECs, ultimately leading to collagen IV deposition and liver fibrosis. Hepatic ECs express several angiocrine factors, such as BMP2, BMP6, Wnt2 and Rspo3, to regulate liver iron metabolism and metabolic zonation. We found that these angiocrine factors were significantly decreased in ECs from *Bmp9/10*$^{\text{HSC-KO}}$ mice, which further resulted in liver iron overload and disruption of HC zonation. In summary, we demonstrated that HSCs play a central role in mediating liver cell–cell crosstalk via the production of BMP9/10 to maintain liver health.

eLife assessment

This **valuable** study delineates the cellular contributions of BMP signaling in liver development and function. The findings are **convincing**, and the study employs state-of-the-art molecular, genetic, and cellular approaches to demonstrate that hepatic stellate cells play a central role in liver health by mediating cell-to-cell crosstalk via the production of specific BMP proteins. This study will be of interest to scientists interested in developmental biology and organ physiology.

Introduction

Almost all organs in vertebrates consist of different cell types that undertake their individual functions to maintain organ homeostasis (1), such as vascular endothelial cells supplying oxygen and nutrients to the organ (2) and immune cells, especially tissue-resident macrophages, constantly clearing cell debris and monitoring tissue microenvironments to prevent pathogen infection (3). Usually, these different cell types originate from distinct progenitors and differentiate into specialized cell types via the expression of lineage-specific transcription factors during development (4). Meanwhile, crosstalk between these individual cells within one organ occurs and promotes them to continue to specialize (5, 6), which is needed for the maintenance of the organotypic phenotypes of these cells. However, the cell–cell communication within organs is largely unknown.

The liver is composed of four major cell types: hepatocytes (HCs), Kupffer cells (KCs), endothelial cells (ECs), and hepatic stellate cells (HSCs). The liver exemplifies the importance of cellular interactions in maintaining organ integrity (7–9). For example, secretion of Wnt signaling and BMP2/6 by ECs functions on hepatocytes to control hepatic zonation and iron metabolism (10–13), respectively. Loss of these signals results in liver dysfunction. Recent advances in RNA-sequencing technology and algorithms have enabled a better understanding of the cellular composition and potential cellular interactions of the liver (14). However, the speculative cues still need experimental validation, and more importantly, it is still unknown what consequences happen if specific cell–cell interactions are interrupted.

HSCs reside in the space of Disse and directly interact with HCs, ECs, and KCs (15). HSCs are well known for their pathological role in liver fibrosis, as HSC activation is a critical step in the development of chronic liver disease (16). However, in addition to the storage of retinoids, the physiological role of HSCs in the normal liver remains unclear. ALK1, encoded by the activin A receptor-like type 1 (*Acvrl1*) gene, is the receptor of BMP9 and BMP10. Its mutations result in hereditary hemorrhagic telangiectasia (HHT), which causes vascular malformations in multiple organs, including the liver (17). It has been reported that liver sinusoidal EC-specific *Alk1*-deficient mice exhibit severe liver vascular malformations (18), which mimic the liver symptoms observed in HHT patients. We and others demonstrated that ALK1 is needed for KC survival and identity, and the ability of KCs from *Alk1*-deficient mice to capture bacteria from the bloodstream was significantly impaired (19, 20). BMP9 is mainly expressed in the liver. Using antibody staining, BMP9 was reported to be expressed in human hepatocytes (21). Recently, based on PCR and scRNA-Seq analysis, BMP9 and BMP10 have been shown to be mainly expressed by murine HSCs (20, 22). However, no study has systematically examined which liver cell types secrete BMP9 and BMP10 and regulate ECs and KCs via these two paracrine factors. Here, we generated mice with conditional knockout of both *Bmp9 and Bmp10* in different liver cell types and found that HSCs are the functional source of BMP9 and BMP10. Interestingly, conditional deletion of *Bmp9/10* from HSCs (*Bmp9/10*$^{HSC\text{-}KO}$) mice not only resulted in loss of KC and EC identity but also affected HC phenotypes in an indirect way, which ultimately resulted in liver dysfunction, suggesting that HSCs play a central role in orchestrating the interactions between different liver cell types under physiological conditions.

Results

HSCs are the functional source of BMP9 and BMP10 in the liver

To generate mice lacking *Bmp9* and *Bmp10* in different liver cell types, $Bmp9^{fl/fl}$ and $Bmp10^{fl/fl}$ mice were prepared and mated with Alb^{Cre}, $Clec4f^{Cre}$, $Tie2^{Cre}$, or $Lrat^{Cre}$ mice, which have been extensively used in the literature to produce HCs, KCs, ECs, and HSC conditional knockout mice (12, 19, 23–25), respectively. Because BMP9 and BMP10 play a redundant role in regulating KCs (19), conditional double knockout mice ($Bmp9^{fl/fl}Bmp10^{fl/fl}Alb^{Cre}$, $Bmp9^{fl/fl}Bmp10^{fl/fl}Tie2^{Cre}$, $Bmp9^{fl/fl}Bmp10^{fl/fl}Clec4f^{Cre}$and $Bmp9^{fl/fl}Bmp10^{fl/fl}Lrat^{Cre}$) were generated. To systematically investigate which liver cell types produce BMP9 and BMP10, we acquired liver tissues from these mice. Quantitative PCR analysis revealed that *Bmp9* and *Bmp10* mRNA expression was significantly reduced in the liver tissues from $Bmp9^{fl/fl}Bmp10^{fl/fl}Lrat^{Cre}$ ($Bmp9/10^{HSC\text{-}KO}$) mice compared to other Cre deleter mice (**Figure 1a**). Using Cre-mediated reporter mice, we demonstrated that $Lrat^{Cre}$ mice can specifically target HSCs (**Figure 1b**). BMP10 is mostly expressed in the heart, followed by the liver (26). However, *Bmp10* expression in the heart was not affected in $Bmp9/10^{HSC\text{-}KO}$ mice (**Figure 1c**). ALK1 is the receptor of BMP9/10. To investigate which liver cell types express ALK1 and respond to BMP9/10, we prepared transgenic ALK1 reporter mice, which can faithfully reflect the expression of ALK1. We found that ALK1 was expressed on ECs and KCs but not HCs and HSCs (**Figure 1d**), suggesting that BMP9/10 can directly function on ECs and KCs via ALK1. Accordingly, we found that surface markers of liver $F4/80^+$ macrophages from $Bmp9/10^{HSC\text{-}KO}$ mice, including CLEC4F, Tim4 and VSIG4, were almost not expressed (**Figure 1e** and **1f**). In contrast, these markers were not affected in the liver $F4/80^+$ macrophages from $Bmp9^{fl/fl}Bmp10^{fl/fl}Alb^{Cre}$, $Bmp9^{fl/fl}Bmp10^{fl/fl}Tie2^{Cre}$ and $Bmp9^{fl/fl}Bmp10^{fl/fl}Clec4f^{Cre}$mice (**Supplementary Figure 1**). LYVE1 and CLEC2, the surface markers of $CD31^+$ hepatic ECs, were also reduced in the livers of $Bmp9/10^{HSC\text{-}KO}$ mice (**Figure 1g**). In addition, we also determined the phenotypes of KCs and ECs from $Bmp10^{fl/fl}Lrat^{Cre}$ mice to exclude the possibility that the altered phenotypes observed in $Bmp9^{fl/fl}Bmp10^{fl/fl}Lrat^{Cre}$mice were due to Cre-mediated cytotoxicity (27) and found that these cells were not affected (**Supplementary Figure 2**). Collectively, these results suggest that HSCs are the functional source of BMP9 and BMP10 in the liver to regulate KCs and ECs.

The differentiation of liver macrophages from $Bmp9/10^{HSC\text{-}KO}$ mice is blocked in a status of monocyte-derived macrophages

To acquire more information about transcriptome changes in liver macrophages in the *Bmp9/10*-deficient liver microenvironment, we performed bulk RNA-seq analysis on sorted liver macrophages from $Bmp9/10^{HSC\text{-}KO}$ mice compared with their controls. We found that 2424 genes were differentially expressed (FC>2, p-adj<0.05), among which 1313 genes were upregulated and 1111 genes were downregulated in liver macrophages from $Bmp9/10^{HSC\text{-}KO}$ mice compared to their control mice (**Figure 2a**). From these differentially expressed genes, we found that genes associated with the identity of KCs, such as *Fabp7*, *Cd5l*, *Cdh5* and *Clec4f*, were significantly downregulated in liver macrophages from $Bmp9/10^{HSC\text{-}KO}$ mice (**Figure 2b**). *Id1* and *Id3*, target genes of ALK1 signaling and important regulators of KC differentiation, were also significantly reduced in liver macrophages from $Bmp9/10^{HSC\text{-}KO}$ mice (**Figure 2b**). We also observed downregulation of embryonic KC marker *Timd4* (encoding Tim4) expression and upregulation of monocytic *Cx3cr1* and *Ccr2* expression in liver macrophages from $Bmp9/10^{HSC\text{-}KO}$ mice (**Figure 2c**), suggesting that embryonic KCs were lost and replaced by monocyte-derived macrophages/KCs, as a reduced number of liver macrophages was observed in $Bmp9/10^{HSC\text{-}KO}$ mice (**Figure 2d**).

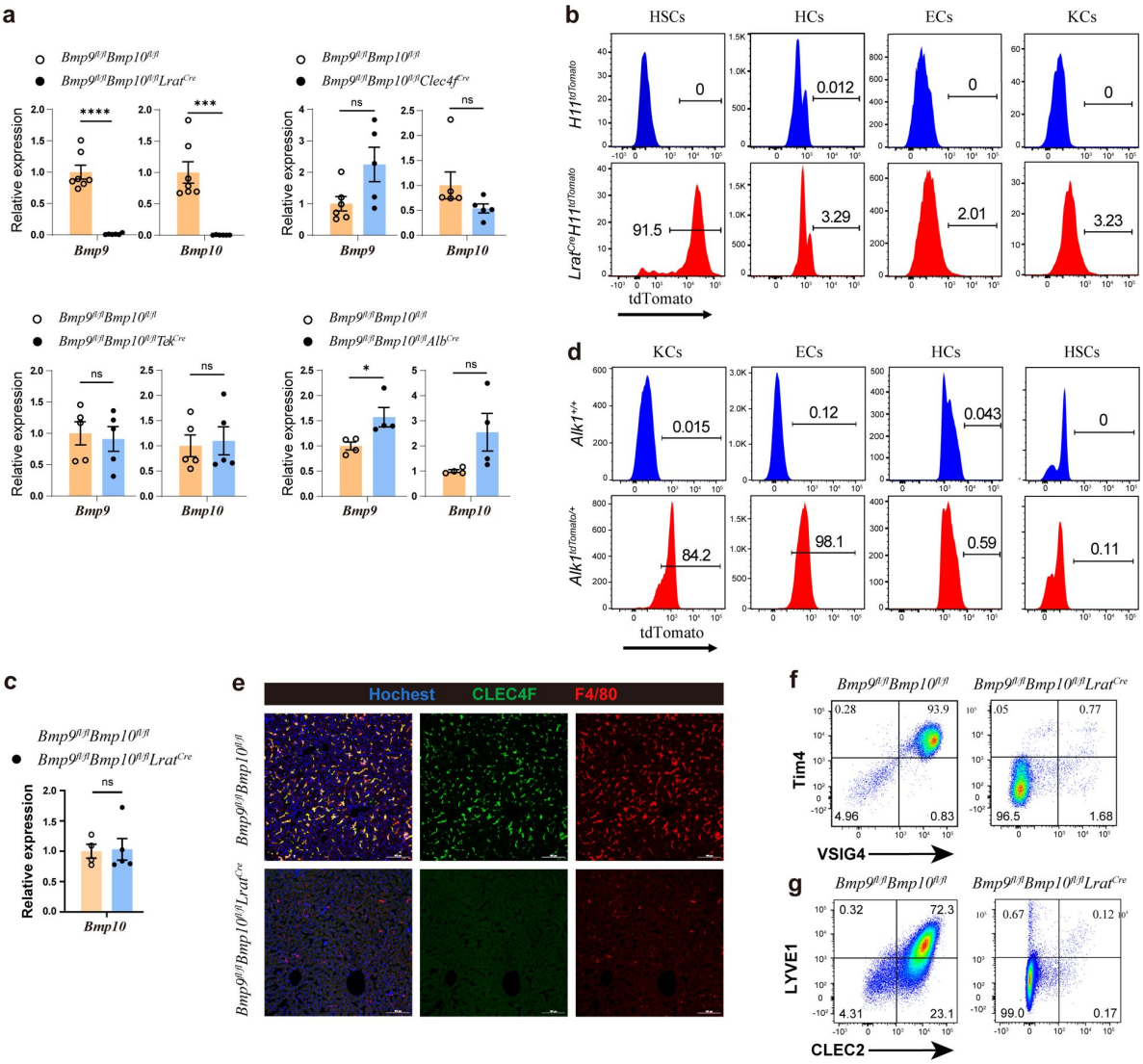

Figure 1.

HSCs are the major source of BMP9 and BMP10 in the liver.

(a) Quantitative PCR analysis of *Bmp9* and *Bmp10* expression in the liver from the indicated mice. (b) Representative flow cytometric expression of tdTomato in HSCs, HCs, ECs, and KCs from $Lrat^{Cre}H11^{tdTomato}$mice (n=3/group). (c) Quantitative PCR analysis of *Bmp10* expression in the right atrium from $Bmp9^{fl/fl}Bmp10^{fl/fl}Lrat^{Cre}$and their littermate controls. (d) Representative flow cytometric expression of tdTomato in HSCs, HCs, ECs, and KCs from $Alk1^{tdTomato}$mice (n=3/group). (e) Representative immunofluorescence images of liver sections from $Bmp9^{fl/fl}Bmp10^{fl/fl}Lrat^{Cre}$ and their littermate controls at the age of 3-12 weeks (n=6/group). Scale bars: 100μm. (f) Representative flow cytometric expression of Tim4 and VSIG4 in KCs from $Bmp9^{fl/fl}Bmp10^{fl/fl}Lrat^{Cre}$ (n=4) and their littermate controls (n=2). (g) Representative flow cytometric expression of LYVE1 and CLEC2 in ECs from $Bmp9^{fl/fl}Bmp10^{fl/fl}Lrat^{Cre}$ (n=3) and their littermate controls (n=3). Results represent the mean ± SEM. *P < 0.05, **P < 0.01, ***P < 0.001, and ****P <0.0001, by 2-tailed Student's t test (a,c).

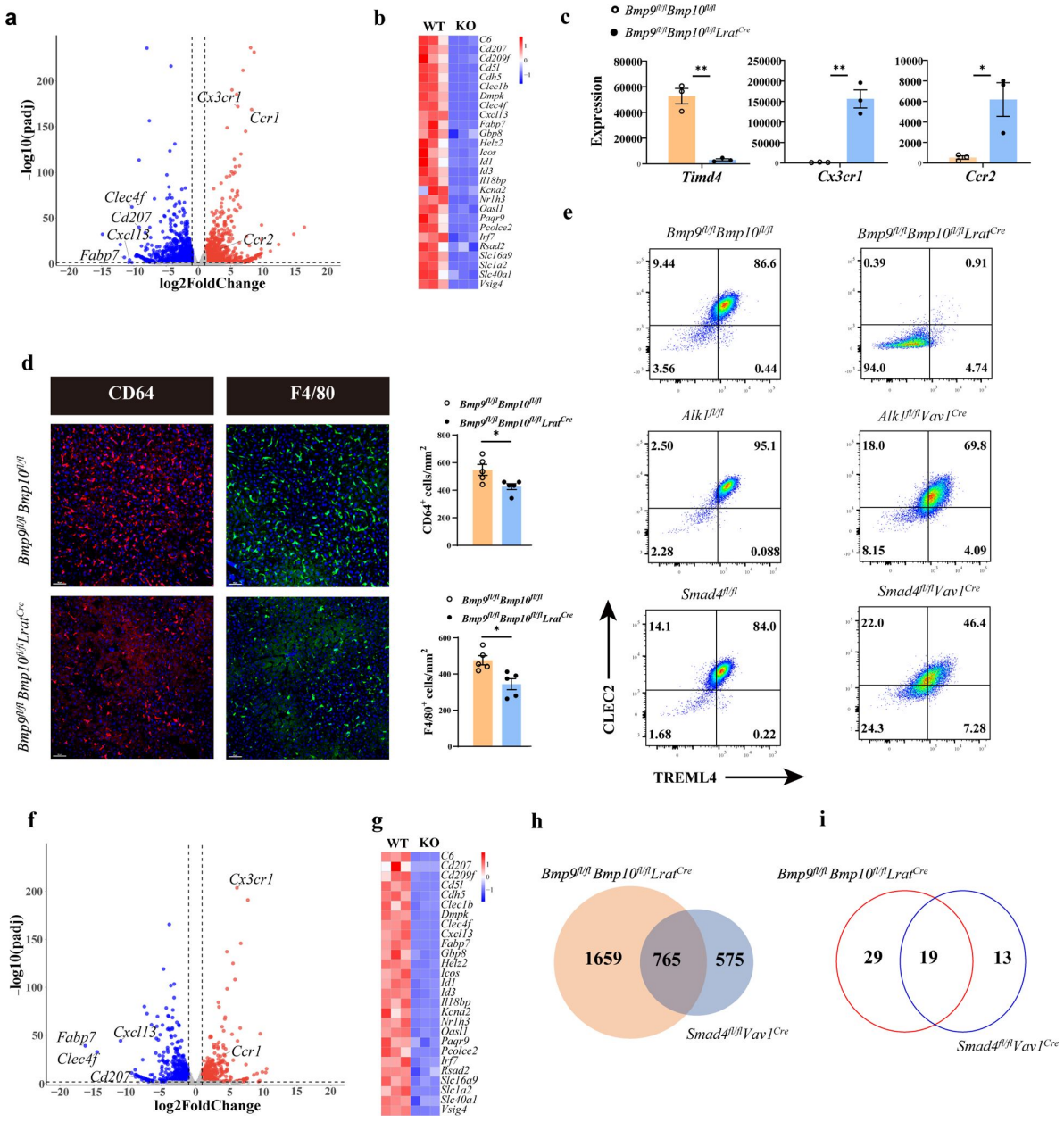

Figure 2.

The differentiation of liver macrophages was inhibited in *Bmp9$^{fl/fl}$Bmp10$^{fl/fl}$Lrat^{Cre}* mice.

(a) Volcano plot of the RNA-seq data of sorted liver macrophages from *Bmp9$^{fl/fl}$Bmp10$^{fl/fl}$Lrat^{Cre}* and control mice. Genes upregulated and downregulated are shown in red and blue, respectively (fold change [FC] > 2, adjusted p[p-adj] < 0.05). (b) Heatmap showing signature genes expressed differentially in liver macrophages from *Bmp9$^{fl/fl}$Bmp10$^{fl/fl}$Lrat^{Cre}* and control mice. (c) Expression counts of indicated genes in liver macrophages from *Bmp9$^{fl/fl}$Bmp10$^{fl/fl}$Lrat^{Cre}* and control mice. (d) Immunofluorescence images of F4/80^{+} and CD64^{+} liver macrophages in sections from *Bmp9$^{fl/fl}$Bmp10$^{fl/fl}$Lrat^{Cre}* mice and their controls. Liver macrophages number was measured (right). (e) Flow cytometric expression of CLEC2 and TREML4 in liver macrophages from the indicated mice (n=3-4/group). (f) Volcano plot of the RNA-seq data of sorted liver macrophages from *Smad4$^{fl/fl}$Vav1^{Cre}* and control mice. Genes upregulated and downregulated are shown in red and blue, respectively (fold change [FC] > 2, adjusted p[p-adj] < 0.05). (g) Heatmap showing signature genes expressed differentially in liver macrophages from *Smad4$^{fl/fl}$Vav1^{Cre}* and control mice. (h, i) Venn diagram showing DE genes (h) and transcription factors (i) specific to liver macrophages of *Bmp9$^{fl/fl}$Bmp10$^{fl/fl}$Lrat^{Cre}*, *Smad4*-deficient liver macrophages or shared between both mac populations. Results represent the mean ± SEM. *P < 0.05, **P <0.01, ***P < 0.001, and ****P <0.0001, by 2-tailed Student's t test (c, d).

Upon KC loss, blood monocytes are recruited into the liver, immediately differentiate into F4/80^{+} monocyte-derived macrophages (MoMs) and then gradually acquire the expression of CLEC2, CLEC4F and VSIG4 to become monocyte-derived KCs (MoKCs) with time (15, 28). CLEC2, encoded by *the Clec1b* gene, was thought to be one of the earliest markers gained by monocyte-derived KCs and can be used to discriminate MoKCs from MoMs (29). In addition, TREML4 expression is immediately upregulated upon blood monocyte entry into the liver (25). Interestingly, we found that nearly all liver macrophages from *Bmp9/10*$^{\text{HSC-KO}}$ mice did not express CLEC2 and TREML4, but liver macrophages from *Alk1*$^{fl/fl}$*Vav1*^{Cre} and *Smad4*$^{fl/fl}$*Vav1*^{Cre} mice did (**Figure 2e**), suggesting that the differentiation of liver macrophages from *Bmp9/10*$^{\text{HSC-KO}}$ mice is completely blocked in a status of monocyte-derived macrophages, and the differentiation defect in liver macrophages from *Bmp9/10*$^{\text{HSC-KO}}$ mice is more pronounced than that from *Alk1*$^{fl/fl}$*Vav1*^{Cre}and *Smad4*$^{fl/fl}$*Vav1*^{Cre} mice. To understand this discrepancy, we performed bulk RNA-seq analysis on sorted liver macrophages from *Smad4*$^{fl/fl}$*Vav1*^{Cre}mice, as Smad4 functions as a common Smad needed for transcriptional regulation in response to ALK signaling. In addition to ALK1, BMP9 and BMP10 also bind ALK2 with low affinity to transduce signals (26). Analysis of the DE genes between *Smad4*-sufficient and *Smad4*-deficient KCs identified 1340 DE genes, including many KC signature genes (**Figure 2f** and **2g**). Comparison of the difference between the DE genes in liver macrophages from *Bmp9/10*$^{\text{HSC-KO}}$ and *Smad4*$^{fl/fl}$*Vav1*^{Cre} mice revealed that 1659 of 2424 DE genes in liver macrophages from *Bmp9/10*$^{\text{HSC-KO}}$ mice did not overlap with DE genes in MoKCs from *Smad4*$^{fl/fl}$*Vav1*^{Cre} mice (**Figure 2h**), which is consistent with the phenomenon described above, indicating that in addition to Smad4, alterations in other molecular mechanisms may affect the phenotypes of liver macrophages in *Bmp9/10*$^{\text{HSC-KO}}$ mice.

Transcription factors play an important role in the differentiation of tissue-resident macrophages. We compared the nonoverlapping transcription factors between the DE genes in liver macrophages from *Bmp9/10*$^{\text{HSC-KO}}$ and *Smad4*$^{fl/fl}$*Vav1*^{Cre} mice and found 29 transcription factors only downregulated in liver macrophages from *Bmp9/10*$^{\text{HSC-KO}}$ mice (**Figure 2i** and **Supplementary Table 1**). Among these transcription factors, we focused on *Rxra* because it has been reported to regulate the development of many embryonic tissue-resident macrophages, including KCs (30), but it is unclear whether RXRa regulates the differentiation of blood monocytes to MoKCs. To test this hypothesis, we prepared *Rxra*$^{fl/fl}$*Csf1r*^{Cre} *Clec4f*^{DTR} mice, in which DT injection can delete KCs and monocytes recruited into the liver to differentiate into liver macrophages, which can be targeted by the *Csf1r*^{Cre} strain to eliminate the *Rxra* gene (**Supplementary Figure 3a**). We found that RXRα deficiency significantly inhibited the differentiation of blood monocytes to MoKCs, as the proportion of CLEC2^{+} and VSIG4^{+} macrophages was significantly reduced in *Rxra*-deficient macrophages compared with their controls (**Supplementary Figure 3b** and **3c**), suggesting that the differentiation defect of liver macrophages from *Bmp9/10*$^{\text{HSC-KO}}$ mice may be partially caused by *Rxra* downregulation.

Endothelial cells from *Bmp9/10*$^{\text{HSC-KO}}$ mice are transdifferentiated into continuous endothelial cells

Next, to understand how ECs were affected in *Bmp9/10*$^{\text{HSC-KO}}$ mice, we performed bulk RNA-seq analysis on sorted CD45^{-}CD31^{+} endothelial cells from *Bmp9/10*$^{\text{HSC-KO}}$ mice compared with their controls. We found that 2692 genes were differentially expressed (FC>2, p-adj<0.05), among which 1534 genes were upregulated and 1158 genes were downregulated in ECs from *Bmp9/10*$^{\text{HSC-KO}}$ mice compared to their control mice (**Figure 3a**). Both GATA4 and MAF act as master regulators of hepatic sinusoidal differentiation (31, 32), and their expression in ECs can be induced by BMP9 *in vitro* (32, 33). In our transcriptomic data, *Gata4* and *Maf* expression in endothelial cells from *Bmp9/10*$^{\text{HSC-KO}}$ mice was significantly reduced compared with that in their controls (**Figure 3b**). Consistent with the phenotypes of *Gata4/Maf*-deficient endothelial cells, the expression of sinusoidal endothelial cell-specific markers such as *Stab 2*, *Fcgr2b* and *Mrc1* was significantly downregulated (**Figure 3c**), while the expression of continuous endothelial cell-

specific markers such as *Cd34*, *Emcn*, *Apln* and *Aplnr* was upregulated in ECs from *Bmp9/10*$^{HSC-KO}$ mice (**Figure 3d**). Immunostaining revealed obviously increased expression of CD34 (**Figure 3e**). Folw cytometry also confirmed the reduced expression of C-Maf (encoded by *Maf*), CD32b (encoded by *Fcgr2b*), CD117 (encoded by *Kit*) and CD206 (encoded by *Mrc1*) (**Figure 3f** and **3 g**). In addition, genes associated with large arteries were significantly upregulated in ECs from *Bmp9/10*$^{HSC-KO}$ mice (**Figure 3h**). These results suggested that hepatic ECs in *Bmp9/10*$^{HSC-KO}$ mice lost their identity and were transdifferentiated into continuous endothelial and large arterial cells.

Liver metabolic zonation and iron metabolism are disrupted in *Bmp9/10*$^{HSC-KO}$ mice

Angiocrine factors Wnts and BMP2/6 signal were shown to control hepatic metabolic zonation and iron metabolism (10–13), respectively. The expression of these genes was significantly reduced in ECs from *Bmp9/10*$^{HSC-KO}$ mice (**Figure 4a**). Prussian blue staining revealed that 5 out of 7 *Bmp9/10*$^{HSC-KO}$ mice showed mild iron overload in the focal liver (**Figure 4b**). Wnt pathway activation induces the expression of zonated proteins such as glutamine synthetase. Immunostaining confirmed the disappearance of glutamine synthetase (GS) in the livers of *Bmp9/10*$^{HSC-KO}$ mice (**Figure 4c**), suggesting that liver metabolic zonation was disrupted in *the Bmp9/10*-deficient liver microenvironment.

To acquire more information regarding how the livers were affected under the condition of BMP9/10 deficiency, we performed bulk RNA-seq analysis on whole liver samples of *Bmp9/10*$^{HSC-KO}$ mice and their control mice at the age of 12 weeks. We analyzed the expression of Wnt signal target genes enriched in the pericentral zone and found that most pericentral Wnt signal targets were significantly downregulated in the livers of *Bmp9/10*$^{HSC-KO}$ mice, including *Glul*, *Oat*, *Cyp2e1*, *Cyp1a2*, *Cldn2*, *Axin2*, *Lect2*, *Lgr5*, *Tbx3* and *Rnf43* (**Figure 4d**), supporting the fact that the liver microenvironment in *Bmp9/10*$^{HSC-KO}$ mice lacks Wnt2, Wnt9b and Rspo3 signaling. In addition, BMP9 and BMP10 play a redundant role in regulating liver metabolic zonation, as glutamine synthetase was still expressed in the livers of *Bmp9*$^{fl/fl}$*Lrat*^{Cre} and *Bmp10*$^{fl/fl}$*Lrat*^{Cre} mice (**Figure 4e** and **4f**).

Liver fibrosis occurs in *Bmp9/10*$^{HSC-KO}$ mice

Liver weight and the liver/body weight ratio were significantly reduced in *Bmp9/10*$^{HSC- KO}$ mice at the age of 12W compared with control mice (**Figure 5a**), suggesting that liver development is impaired. Picrosirius red staining revealed increased collagen deposition in the livers of *Bmp9/10*$^{HSC-KO}$ mice at the age of 12W (**Figure 5b**), suggesting that these mice presented liver fibrosis. PDGFB is a profibrotic cytokine that results in HSC activation and liver fibrosis. In the transcriptomic data, we found that *Pdgfb* was significantly upregulated in the liver tissue, ECs and liver macrophages of *Bmp9/10*$^{HSC-KO}$ mice (**Figure 5c**). Immunostaining revealed that the expression of desmin and type I collagen, two markers of HSC activation, was upregulated in the liver tissues of *Bmp9/10*$^{HSC-KO}$ mice (**Figure 5d**), suggesting that HSC activity was increased. Endothelial Gata4 deficiency leads to sinusoidal capillarization (34). In line with this report, the expression of collagen IV, a marker of EC capillarization, was significantly increased in the livers of *Bmp9/10*$^{HSC-KO}$ mice, as revealed by immunostaining (**Figure 5e**) and the transcriptomic data of ECs (**Figure 5f**). These results suggested that liver fibrosis in *Bmp9/10*$^{HSC-KO}$ mice was due to EC capillarization and HSC activation.

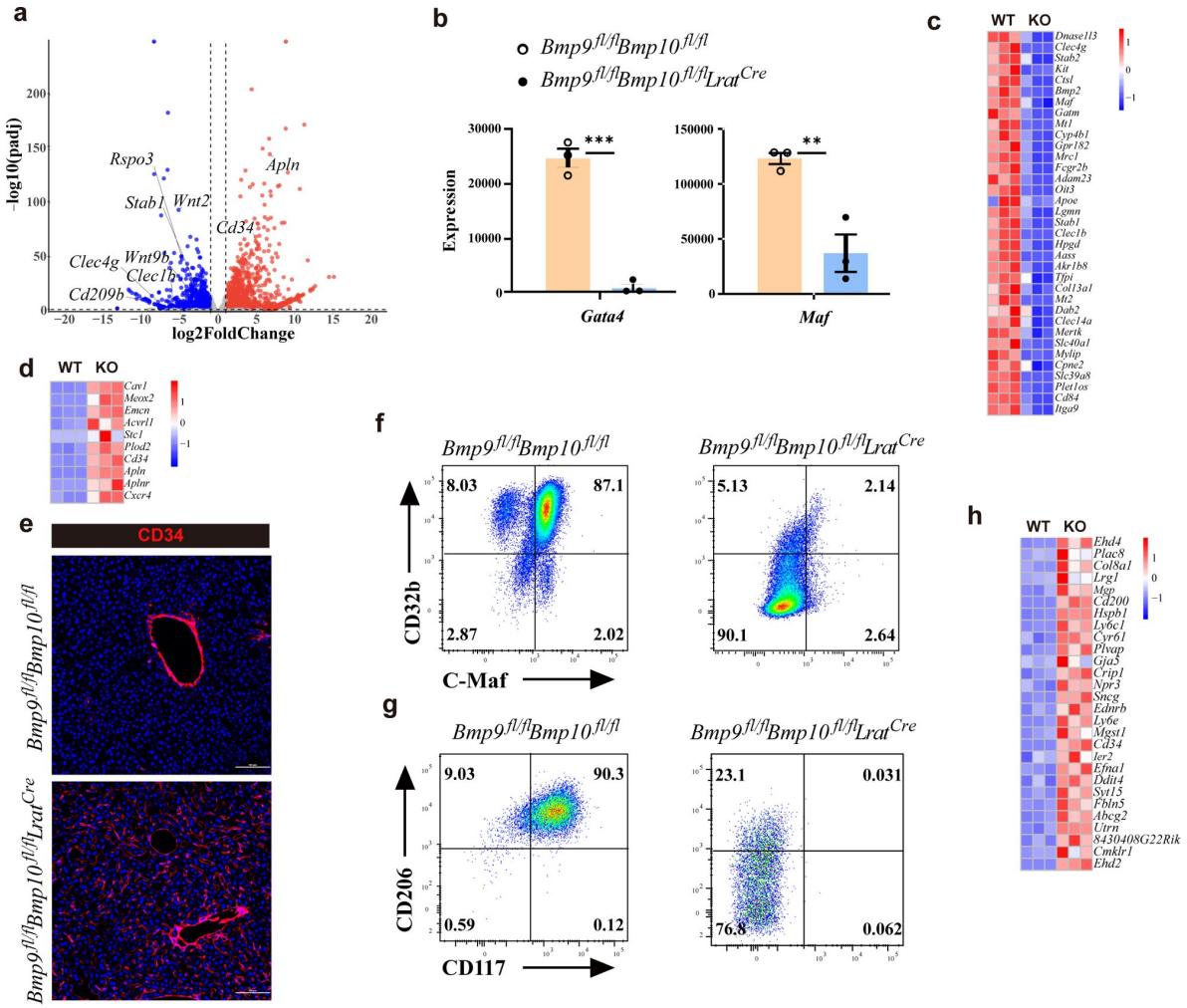

Figure 3.

Endothelial cells from *Bmp9*$^{fl/fl}$*Bmp10*$^{fl/fl}$*Lrat*^{Cre} mice are transdifferentiated to continuous endothelial cells.

(a) Volcano plot of the RNA-seq data of sorted hepatic ECs from *Bmp9*$^{fl/fl}$*Bmp10*$^{fl/fl}$*Lrat*^{Cre}and control mice. Genes upregulated and downregulated are shown in red and blue, respectively (fold change [FC] > 2, adjusted p[p-adj] < 0.05). (b) Expression counts of Gata4 and Maf genes in ECs from *Bmp9*$^{fl/fl}$*Bmp10*$^{fl/fl}$*Lrat*^{Cre}and control mice. (c, d) Heatmap showing sinusoidal EC-associated genes (c) and continuous EC-associated genes (d) expressed differentially in hepatic ECs from *Bmp9*$^{fl/fl}$*Bmp10*$^{fl/fl}$*Lrat*^{Cre} and control mice. (e) Representative immunofluorescence images in liver sections from *Bmp9*$^{fl/fl}$*Bmp10*$^{fl/fl}$*Lrat*^{Cre} and control mice (n=4/group). Scale bars: 100μm. (f, g) Flow cytometric expression of CD32b, C-Maf, CD206 and CD117 in hepatic ECs from *Bmp9*$^{fl/fl}$*Bmp10*$^{fl/fl}$*Lrat*^{Cre}and littermate controls (n=4-5/group). (h) Heatmap showing the indicated genes expressed differentially in hepatic ECs from *Bmp9*$^{fl/fl}$*Bmp10*$^{fl/fl}$*Lrat*^{Cre} and control mice. Results represent the mean ±SEM. *P < 0.05, **P < 0.01, ***P < 0.001, and ****P <0.0001, by 2-tailed Student's t test (b).

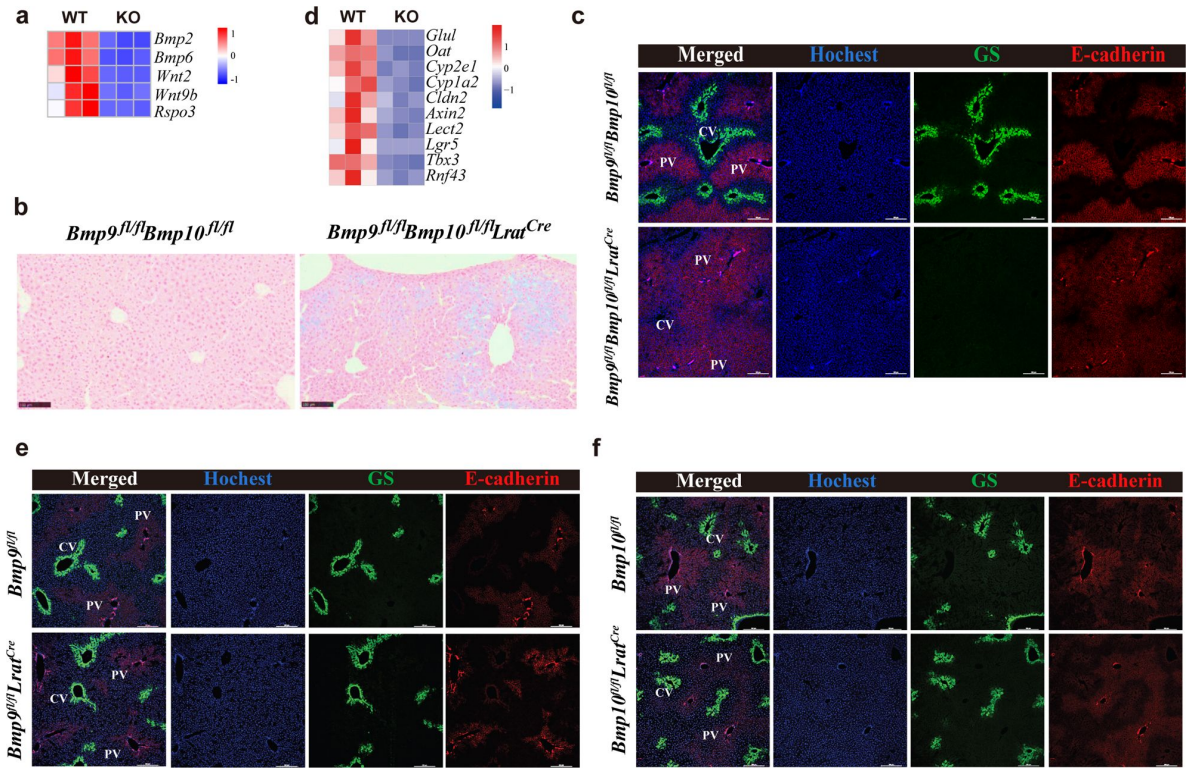

Figure 4.

Liver metabolic zonation and iron metabolism are disrupted in *Bmp9$^{fl/fl}$Bmp10$^{fl/fl}$Lrat^{Cre}* mice.

(a) Heatmap showing the indicated genes expressed differentially in hepatic ECs from *Bmp9$^{fl/fl}$Bmp10$^{fl/fl}$Lrat^{Cre}* and control mice. (b) Prussian blue in livers from *Bmp9$^{fl/fl}$Bmp10$^{fl/fl}$Lrat^{Cre}* mice and their controls. (c) Representative immunofluorescence images in liver sections from *Bmp9$^{fl/fl}$Bmp10$^{fl/fl}$Lrat^{Cre}* mice and their controls (n=5/group). Scale bars: 200μm. (d) Heatmap showing the indicated genes expressed differentially in liver tissues from *Bmp9$^{fl/fl}$Bmp10$^{fl/fl}$Lrat^{Cre}* and control mice at the age of 12W. (e, f) Representative immunofluorescence images in liver sections from *Bmp9$^{fl/fl}$Lrat^{Cre}* (e) and *Bmp10$^{fl/fl}$Lrat^{Cre}*(f) mice and their controls (n=2/group). Scale bars: 200μm.

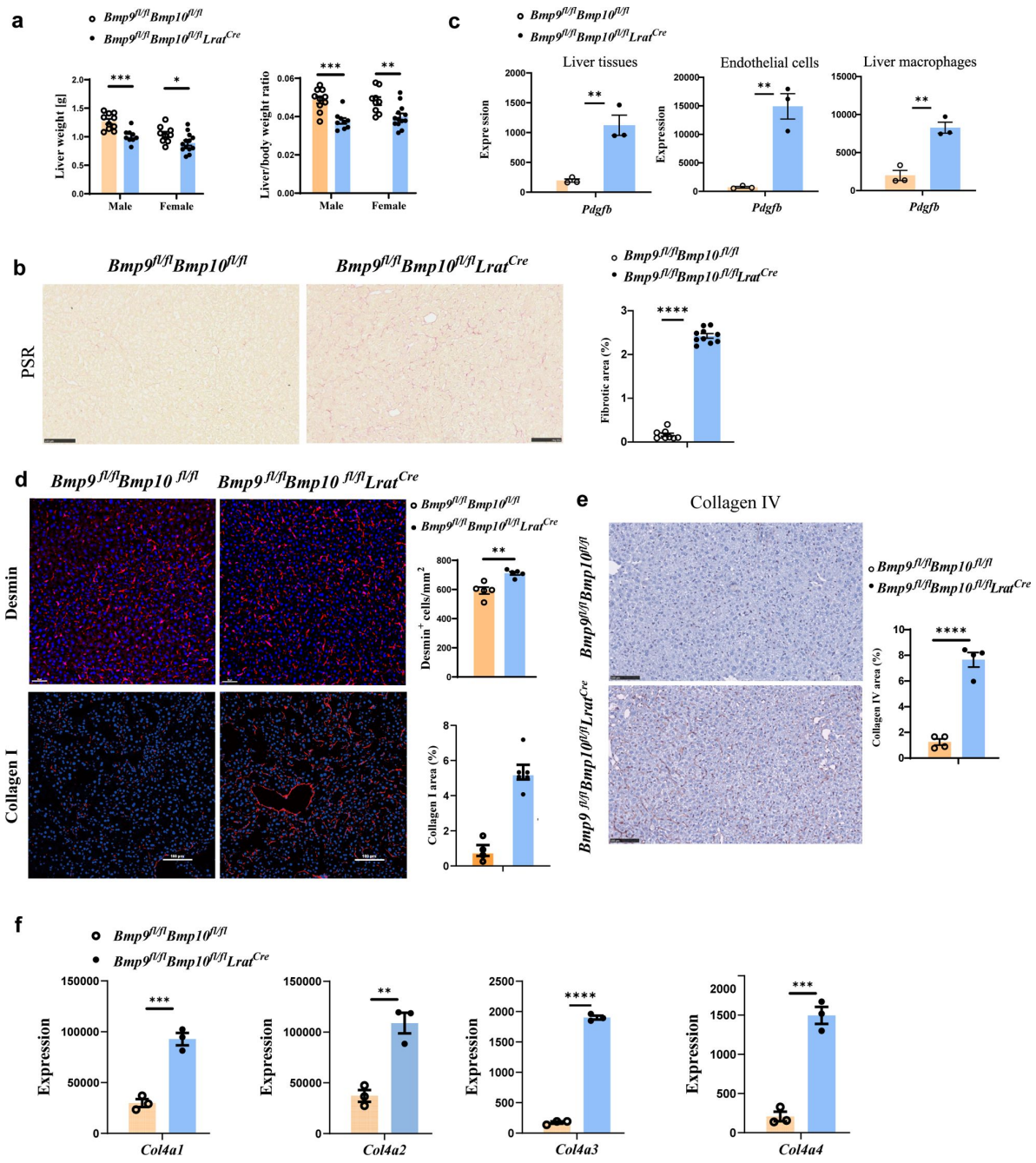

Figure 5.

Liver fibrosis occurs in *Bmp9*$^{fl/fl}$*Bmp10*$^{fl/fl}$*Lrat*^{Cre} mice.

(a) Liver weight and liver to body weight ratio of *Bmp9*$^{fl/fl}$*Bmp10*$^{fl/fl}$*Lrat*^{Cre}mice and their littermate controls at the age of 12W. (b) PSR staining of liver sections from *Bmp9*$^{fl/fl}$*Bmp10*$^{fl/fl}$*Lrat*^{Cre}mice and their controls. Scale bars: 100μm. (c) Expression counts of *Pdgfb* gene in liver tissues (left), endothelial cells (middle) and liver macrophages (right) from *Bmp9*$^{fl/fl}$*Bmp10*$^{fl/fl}$*Lrat*^{Cre}mice and their control mice. (d) Immunofluorescence images of Desmin and collagen I in liver sections in liver tissues from *Bmp9*$^{fl/fl}$*Bmp10*$^{fl/fl}$*Lrat*^{Cre}(12-28W) and control mice. (e) Collagen IV immunohistochemistry staining of liver sections from *Bmp9*$^{fl/fl}$*Bmp10*$^{fl/fl}$*Lrat*^{Cre}mice and their controls. Scale bars:100μm. (f) Expression counts of indicated genes in endothelial cells from *Bmp9*$^{fl/fl}$*Bmp10*$^{fl/fl}$*Lrat*^{Cre}and control mice. Results represent the mean± SEM. *P < 0.05, **P < 0.01, ***P < 0.001, and ****P <0.0001, by 2-tailed Student's t test (a-f).

Discussion

In this study, we demonstrated that HSCs convey BMP9/10 signals to KCs and ECs to maintain their identity. Loss of BMP9/10 in the liver microenvironment resulted in liver macrophage differentiation defects and a shift in hepatic EC differentiation toward continuous ECs and large arterial cells. Under this condition, physiological crosstalk between ECs and HCs was disrupted, which ultimately altered the whole liver microenvironment and resulted in liver dysfunction.

Recently, we and others have demonstrated that ALK1 is essential for KC differentiation, self-renewal, identity, and endocytic ability (19, 20). Here, we undertook systematic genetic manipulation to scrutinize the functional source of BMP9/10 in the liver. We found that instead of ECs, KCs and HCs, HSCs are the predominant source of BMP9/10 critical for KC homeostasis. BMP9 is mainly expressed in the liver, whereas BMP10 is mostly expressed in the heart and weakly expressed in the liver. We found that BMP10 expression in the heart was not affected in *Bmp9/10*$^{\text{HSC-KO}}$ mice, suggesting that the BMP10 signal needed for KCs and ECs was provided by the local liver rather than circulating BMP10 secreted by the heart. Indeed, ALK1 is weakly expressed in KCs and ECs, as the fluorescence signal emitted by KCs and LSECs from *Alk1*^{tdTomato} reporter mice was weak when detected by flow cytometry, suggesting that the concentration of circulating BMP10 may not be enough to activate ALK1 signaling on hepatic ECs and KCs to maintain their phenotypes.

Recently, Schmid et al. used *Stab 2*^{Cre} mice to delete *Alk1* in liver sinusoidal ECs to model liver HHT (18). They found that upon deletion of *Alk1*, liver sinusoidal ECs lost their identity and were transdifferentiated into large arterial cells. In addition, angiocrine Wnt signaling, such as Wnt2, Wnt9b, and Rspondin3, was impaired in *Alk1*-deficient liver sinusoidal ECs, leading to the disruption of liver metabolic zonation (18). These phenomena were also observed in the *Bmp9/10*$^{\text{HSC-KO}}$ mouse model. However, liver fibrosis observed in HHT patients did not occur in the livers of *Alk1*$^{fl/fl}$*Stab 2*^{Cre} mice (18). Indeed, our transcriptomic data showed that *Stab 2* expression was significantly reduced in hepatic ECs of *Bmp9/10*$^{\text{HSC-KO mice}}$, which was consistent with the data from *Bmp9* KO 129/Ola mice (33), suggesting that ALK1 signaling regulated STAB2 expression. Thus, it is possible that heterozygosity for the *Alk1* deletion in ECs may result in reduced expression of STAB2, and the expression of Cre recombinase driven by the *Stab 2* promoter accordingly decreases, so that the *Alk1*-floxed allele in ECs cannot be efficiently deleted by Cre-mediated cyclization, which may explain why liver fibrosis did not occur in *Alk1*$^{fl/fl}$*Stab 2*^{Cre} mice. In view of liver fibrosis, *Bmp9/10*$^{\text{HSC-KO}}$ mice may be a better mouse model to mimic the liver pathology observed in HHT patients (33). In addition, the liver macrophage niche is composed of HCs, ECs and HSCs (15, 25). Thus, the altered phenotypes of HCs and ECs from *Bmp9/10*$^{\text{HSC-KO}}$ mice may be another reason for the differentiation defect of liver macrophages observed in *Bmp9/10*$^{\text{HSC-KO}}$ mice.

Gata4-deficient mice spontaneously develop liver fibrosis (34). Single-cell RNA-seq analysis of healthy and cirrhotic human liver samples revealed that *Gata4* expression was also reduced in ECs from cirrhotic human liver samples (34), suggesting that reduced expression of *Gata4* may contribute to murine and human liver fibrosis. Given that BMP9/10 regulated the expression of *Gata4* in murine ECs, it is possible that the reduced expression of GATA4 may be due to low expression of BMP9/10 in liver cirrhosis. However, the expression of *Bmp9/10* was not detected by single-cell RNA-seq of either healthy or cirrhotic human livers (35–38) due to the low abundance of *Bmp9/10* mRNA in HSCs. Thus, the correlation between *Bmp9/10* expression and liver fibrosis needs further investigation.

Collectively, we demonstrated that BMP9/10 sourced from HSCs function on KCs and ECs to maintain their identity, which further directs HCs to wire metabolic function to meet the organ's needs. Upon disruption of this crosstalk, liver dysfunction ensued. This work illustrates the complexity underlying the crosstalk between different liver cell types.

Methods

Mice

Bmp9^{fll+} (Stock No: T026617), *Bmp10*$^{fll+}$(Stock No: T008480), *Tie2*^{Cre} (Stock No: T003764), *Lrat*^{Cre} (Stock No: T006205) and H11 reporter mice (Stock No: T006163) were obtained from GemPharmatech (Nanjing, China). *Alk1*^{tdTomato} mice that an expression cassette encoding tdTomato and a self-cleaving 2A peptide was inserted into the start codon of *Alk1* gene were prepared by MODEL ORGANISMS (Shanghai, China). *Alb*^{Cre} mice (Stock No: 003574) and *Csf1r*^{Cre} (Stock No: 029206) mice were obtained from Jackson Laboratory. *Smad4*$^{fl/fl}$ and *R26*^{YFP} mice were kindly provided by Dr. Xiao Yang (Beijing Institute of Lifeomics). *Alk1*$^{fl/fl}$ mice were kindly provided by Dr. Zhihong Xu (Fudan University, Shanghai). *Vav1*^{Cre} mice were kindly provided by Dr. Bing Liu (Fifth Medical Center of Chinese PLA General Hospital). *Clec4f*$^{Cre/DTR}$strain mice were established by Nanjing BioMedical Research Institute of Nanjing University (NBRI) using CRISPR/Cas9-mediated genome editing on a C57/BL/6J background. Mice and their littermates were used between eight- to sixteen-week-old unless otherwise specifically indicated. All mice were maintained at the SPF facilities of the Beijing Institute of Lifeomics. All experimental procedures in mice were approved by the Institutional Animal Care and Use Committee at the Beijing Institute of Lifeomics.

Liver cell suspension preparations, flow Cytometry and antibodies

Briefly, the liver was perfused with approximately 20 ml HBSS containing heparin and EDTA, followed by perfusion with digestion buffer containing collagenase type IV (Sigma) and DNase I (Sigma) for 5 min. The digested livers were then disrupted, and pipetted up and down, and the cell suspension was filtered through a 70μm cell strainer. Parenchymal cells were separated from nonparenchymal cells by centrifugation at 50g for 5 min for two times. ECs and liver macrophages were further enriched by iodixanol gradient (OptiPrep) as previously described (39).

Cells were first blocked by anti-CD16/32 antibody and then stained with other appropriate antibodies at 4°C for 20-30 min. 7AAD (559525, BD) was added to dead cell exclusion. Flow cytometry was conducted using an LSRII Fortessa (Becton Dickinson/BD Biosciences). The acquired data were analyzed with FlowJo software (Tree Star). To sort cell, FACSAria III (BD Biosciences) was used. The following antibodies against mouse proteins were used: anti-CD16/CD32 (2.4G2, TONBO Bioscience), anti-CD45 (30-F11, Biolegend), anti-Ly6C (HK1.4, eBioscience), anti-Ly6G (1A8-Ly6g, eBioscience), anti-CD115 (AFS98, Biolegend), anti-CD64 (x54-5/7.1, BioLegend), anti-F4/80 (BM8, Biolegend), anti-Tim4 (RMT4-54, Biolegend), anti-VSIG4 (NLA14, eBioscience), anti-CD31 (390, Biolegend), anti-CD61 (2C9.G2, Biolegend), anti-CD11b (M1/70, Biolegend), anti-LYVE1 (ALY7 Invitrogen), anti-Treml4 (16E5, Biolegend), anti-CLEC2 (17D9/CLEC-2, Biolegend), anti-CD117 (2B8, Biolegend), anti-CD206 (C068C2, Biolegend), anti-c-Maf (sym0F1, Invitrogen), CD32b (AT130-2, Invitrogen). These antibodies were purchased from eBioscience, Biolegend, TONBO Bioscience, Invitrogen and R&D. Secondary antibody donkey anti-goat IgG was purchased from Invitrogen. The gating strategies for KCs, ECs, HSCs, and HCs were shown in **Supplementary figure 4**.

Quantitative Real-Time PCR

Total RNA was isolated with Trizol (Thermo) and cDNA was synthesized with Prime Script RT Reagent Kit (Takara). Quantitative PCR was performed with a SYBR Green PCR kit (Toyobo, Japan) in CFX Connect Real-time PCR detection system (Bio-Rad). The specific qPCR primers used are

listed in **Supplemental Table 2**.

RNA-seq analysis

Total RNA of ECs and liver macrophages was isolated with RNeasy plus Mini Kit (Qiagen). Total RNA of the liver tissues was extracted with Trizol (Thermo). Library preparation was performed with UltraTM RNA Library Prep Kit (Illumina) followed by RNA sequencing using NovaSeq 6000 (Illumina). All samples passed quality control based on the results of FastQC. Reads were aligned to the mouse genome assembly mm10.GRCm38 using HISAT2. The aligned reads were counted using FeatureCounts. Differentially expressed genes were determined with DESeq2 program at p-adj (adjusted p value) < 0.05 and logFC (log fold change) > 1 or logFC where indicated. All RNA sequencing experiments were performed with three independent biological replicates. The heatmap and volcano maps of DEGs were visualized using the “ggplot2” and “pheatmap” R package.

Immunohistochemistry and Immunofluorescence

For immunohistochemistry, the livers were fixed in 4% PFA for 12 hours, and then was dehydrated with gradient ethanol and embedded in paraffin. Sections (4μm) were cut on a Finesse 325 (Thermo Scientific) and adhered to adhesion microscope slides. The paraffin sections were dewaxed and hydrated with xylene and gradient ethanol, and then boiled with antigen retrieval solution to repair antigen. Endogenous peroxidase was blocked with 0.3% hydrogen peroxide for 30 minutes. Paraffin sections were blocked with phosphate-buffered saline (PBS) containing 3% horse serum for 1h, and incubated with Avidin and Biotin for 15 minutes, followed by staining with anti-Collagen IV antibody (ab19808, Abcam) overnight at 4°C. Sections were incubated with secondary antibody, ABC reagent and NovaRed peroxidase substrate of Vector-kit (Vector Laboratories) following with the manufacture. Images were acquired on a C10730-12 NanoZoomer with a 20× /NA 0.75 objective lens.

For immunofluorescence, the fixed livers were dehydrated in PBS solutions containing 15% and 30% sucrose for 12 hours, and embedded in OCT compound (Sakura Finetek). The samples were cut into 20-micron slices using the Cryotome FSE (Thermo Scientific) and then attached to Adhesion Microscope slides. Frozen liver sections were then blocked for 2 hours with 1% bovine serum albumin, 0.3 M glycine, and 10% donkey or goat serum before being stained overnight at 4°C with primary antibodies diluted in PBS with 0.2% Tween, secondary antibodies, and Hoechst for 2h at room temperature. Sections were mounted with Fluoromount G (YEASEN) and images were acquired on a Nikon A1R plus N-STORM confocal microscope with a 10x/0.45 PLANAPO, 20X/0.75 PLANAPO or 40X/0.75 PLANFLUOR objective lens. Laser excitation wavelengths of 405 nm, 488 nm, 561 nm, and 647 nm channels were used for sample fluorescence detection. The following antibodies were used, anti-F4/80 (BM8, Biolegend), anti-CD64 (x54-5/7.1, Biolegend), anti-E-Cadherin (147307, Biolegend), anti-CD34 (RAM34, Invitrogen), anti-Glutamine Synthetase (ab49873, Abcam), anti-Desmin (ab15200, Abcam), anti-type I collagen (ab21286, Abcam), and anti-Clec4F (AF2784, R&D systems). Fluorescent-conjugated secondary antibodies were purchased from Jackson ImmunoResearch Laboratories, Abcam and Invitrogen, as donkey anti rabbit AF594 (711-585-152, Jackson), donkey anti-rat AF488 (ab150153, Abcam), donkey anti-rat AF594 (A21209, Invitrogen) and donkey anti goat FITC (A11055, Invitrogen).

Hematoxylin & eosin (H&E), Picrosirius red (PSR), Nile red and Prussian blue were performed according to standard protocols.

Image processing and analysis

Quantitative analyses of all images were measured using the Fiji package for ImageJ software (NIH) and the Imaris (Oxford Instruments). For coverage measurements of KCs and HSCs, surface modules in Imaris were used to create CD64 and F4/80 biomarkers. A threshold was determined by

the algorithm for background subtraction and manually set to match the cell signals. The number of cells per unit area was accessed by parameters in Imaris. IHC and Picrosirius red staining can be assessed by color deconvolution and the thresholding tool in ImageJ.

Statistics

Data are presented as mean ±s.e.m. All statistics analyses were performed in GraphPad Prism (GraphPad Software). Statistical significance was assessed by unpaired, two-tailed, Student's t-test. *p < 0.05; **p < 0.01; ***p < 0.001; ns, not significant. Each symbol represents an individual mouse. Number of animals is indicated as "n".

Data availability

The raw RNA-seq data generated from this study have been deposited in NCBI's Gene Expression Omnibus (GEO) under accession number GSE244429.

Author contributions

Z.D., conceived the study, designed and performed the experiments, analyzed flow cytometry data, curated results, wrote the manuscript and made figure panels. H.Z., and L.X., performed the experiments, analyzed the data, and visualized images. W.H., performed bioinformatics analysis and made figure panels. W.Y., L.D., Y.T., Y.S., H.C., and H.Y., provided technical support. T. L., conceived the study, edited the manuscript, funding acquisition and supervised the study.

Acknowledgements

This work was supported by the National Science Fund for Distinguished Young Scholars of China (82225009) and National Natural Science Foundation of China (32270941). We thank Flow Cytometry Facility, Animal Facility (Mr. Chen Qiu) and Imaging Facility of National Center for Protein Sciences. Beijing (NCPSB) for their assistance.

Declaration of interests

The authors declare no competing interests.

References

1. Regev A, Teichmann SA, Lander ES, Amit I, Benoist C, Birney E, Bodenmiller B, et al. (2017) **The Human Cell Atlas** *Elife* **6**

2. Wong BW, Marsch E, Treps L, Baes M, Carmeliet P (2017) **Endothelial cell metabolism in health and disease: impact of hypoxia** *EMBO J* **36**:2187–2203

3. Okabe Y, Medzhitov R (2016) **Tissue biology perspective on macrophages** *Nat Immunol* **17**:9–17

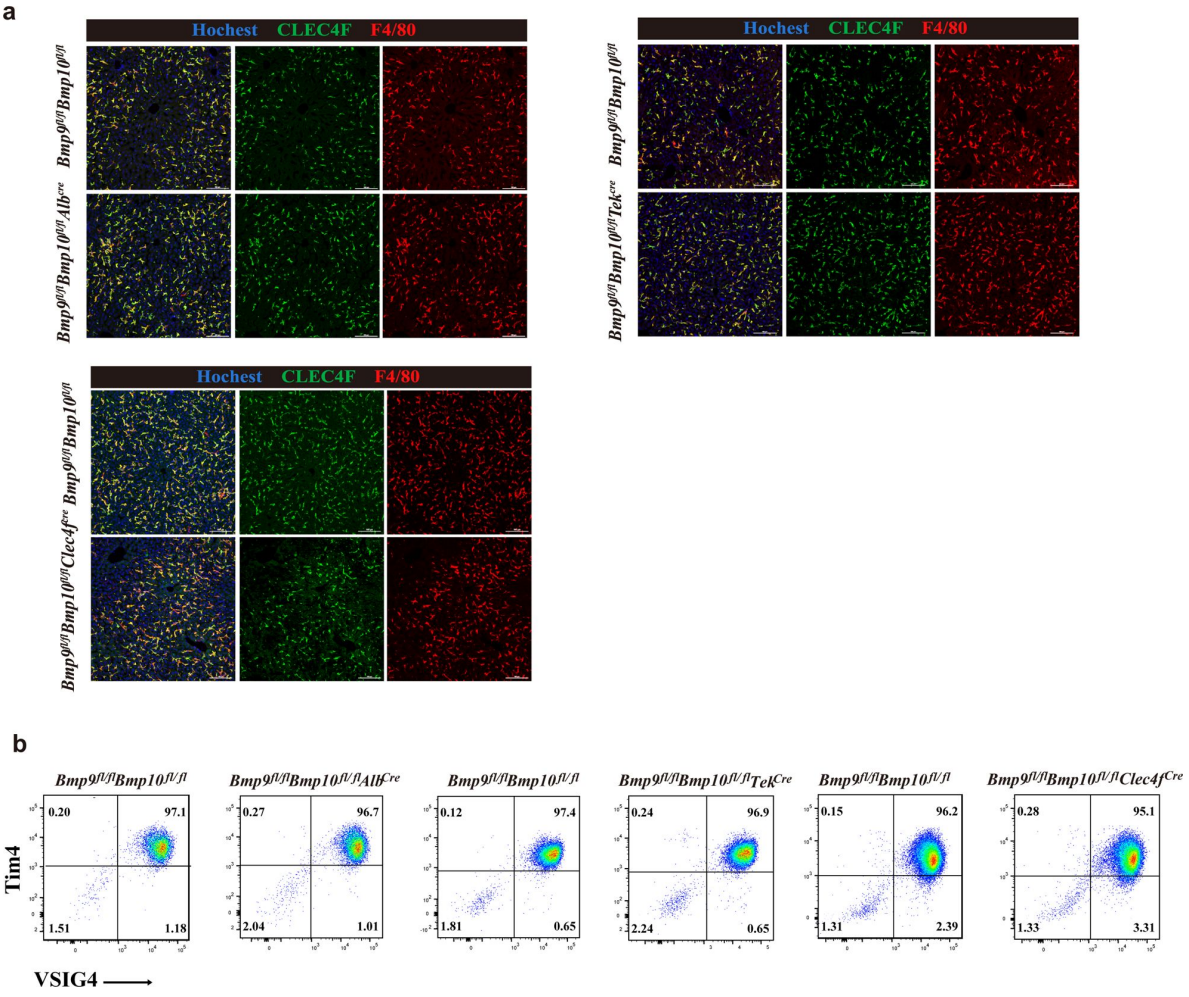

Supplementary Figure 1.

The phenotypes of KCs were not affected in the liver from *Bmp9$^{fl/fl}$Bmp10$^{fl/fl}$Alb^{Cre}*, *Bmp9$^{fl/fl}$Bmp10$^{fl/fl}$Tek^{Cre}* and *Bmp9$^{fl/fl}$Bmp10$^{fl/fl}$Clec4f^{Cre}* mice.

(a) Representative immunofluorescence images of liver sections from the indicated mice (n=3-5/group). Scale bars: 100μm.
(b) Representative flow cytometric expression of Tim4 and VSIG4 in KCs from the indicated mice (n=3-5/group).

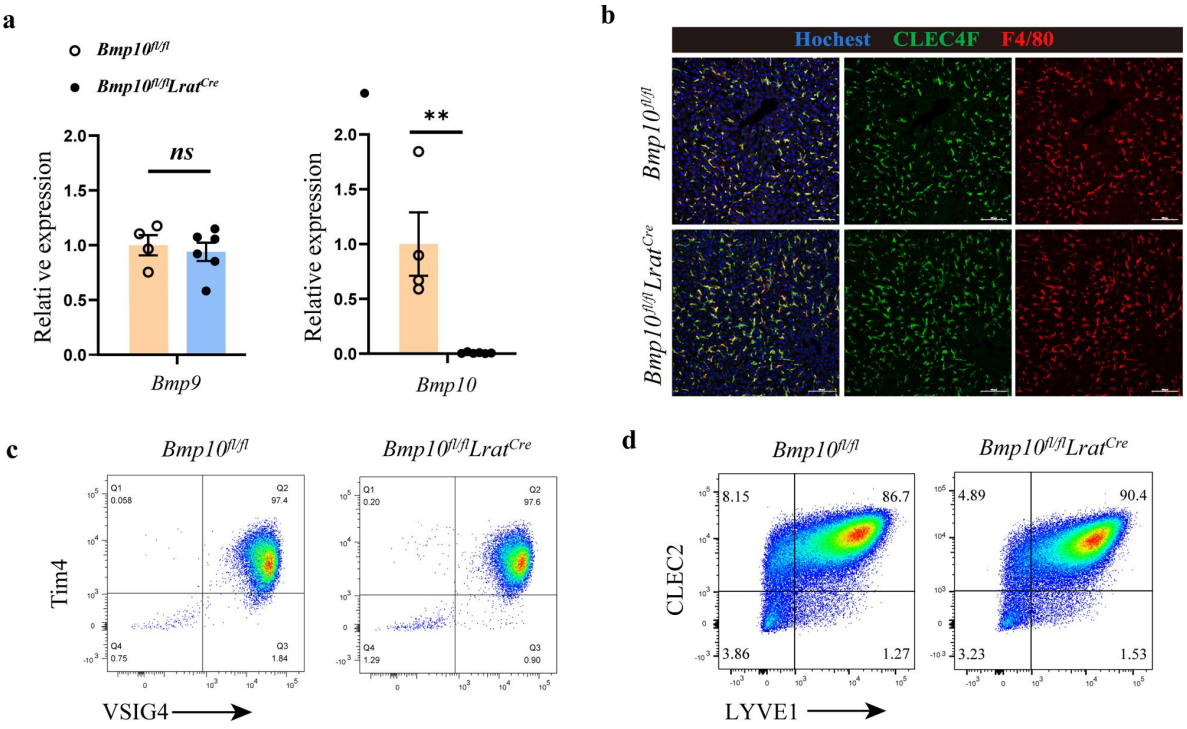

Supplementary Figure 2.

BMP10 can compensate the role of BMP9 in the liver.

(a) Quantitative PCR analysis of *Bmp9* and *Bmp10* expression in the liver from *Bmp10*$^{fl/fl}$*Lrat*^{Cre} and their littermate controls. (b) Representative immunofluorescence images of liver sections from the indicated mice (n=4/group). Scale bars: 100μm. (c-d) Representative flow cytometric expression of the indicated markers in KCs (c) and ECs (d) from *Bmp10*$^{fl/fl}$*Lrat*^{Cre} and their littermate controls (n=2/group). Results represent the mean ± SEM. *P < 0.05, **P < 0.01, 0.0001, by 2-tailed Student's t test (a).

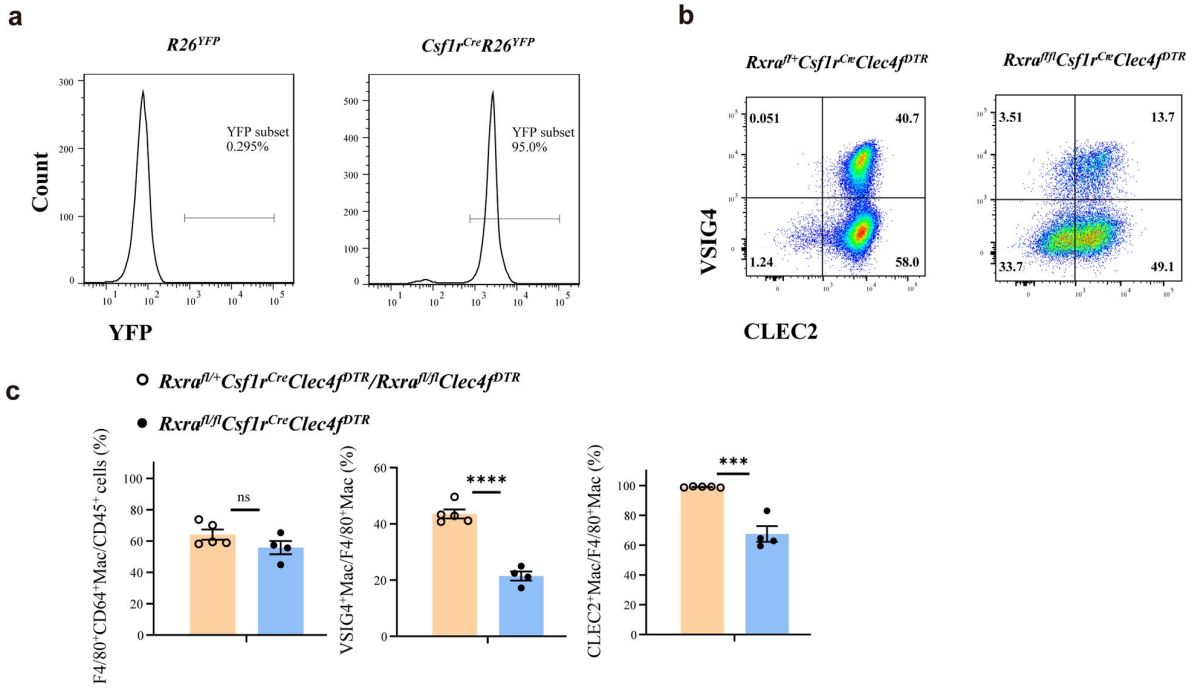

Supplementary Figure 3.

RXRα is required for the differentiation from blood monocytes to MoKCs.

(a) Representative flow cytometric expression of YFP in blood monocytes from *Csf1r*^{Cre}*R26*^{YFP} and control mice (n=2/group). (b,c) Representative flow cytometric expression (b) of CLEC2 and VSIG4 in liver macrophages, and percentage (c) of F4/80^{+}, VSIG4^{+} and CLEC2^{+} liver macrophages from *Rxra*$^{fl/fl}$*Csf1r*^{Cre}*Clec4f*^{DTR} mice and controls. The indicated mice were injected with 200ng/mice diphtheria toxin via IP. After 7 days, VSIG4 and CLEC2 expression in liver macrophages were assessed. Results represent the mean ± SEM. *P < 0.05, **P < 0.01, 0.0001, by 2-tailed Student's t test (B).

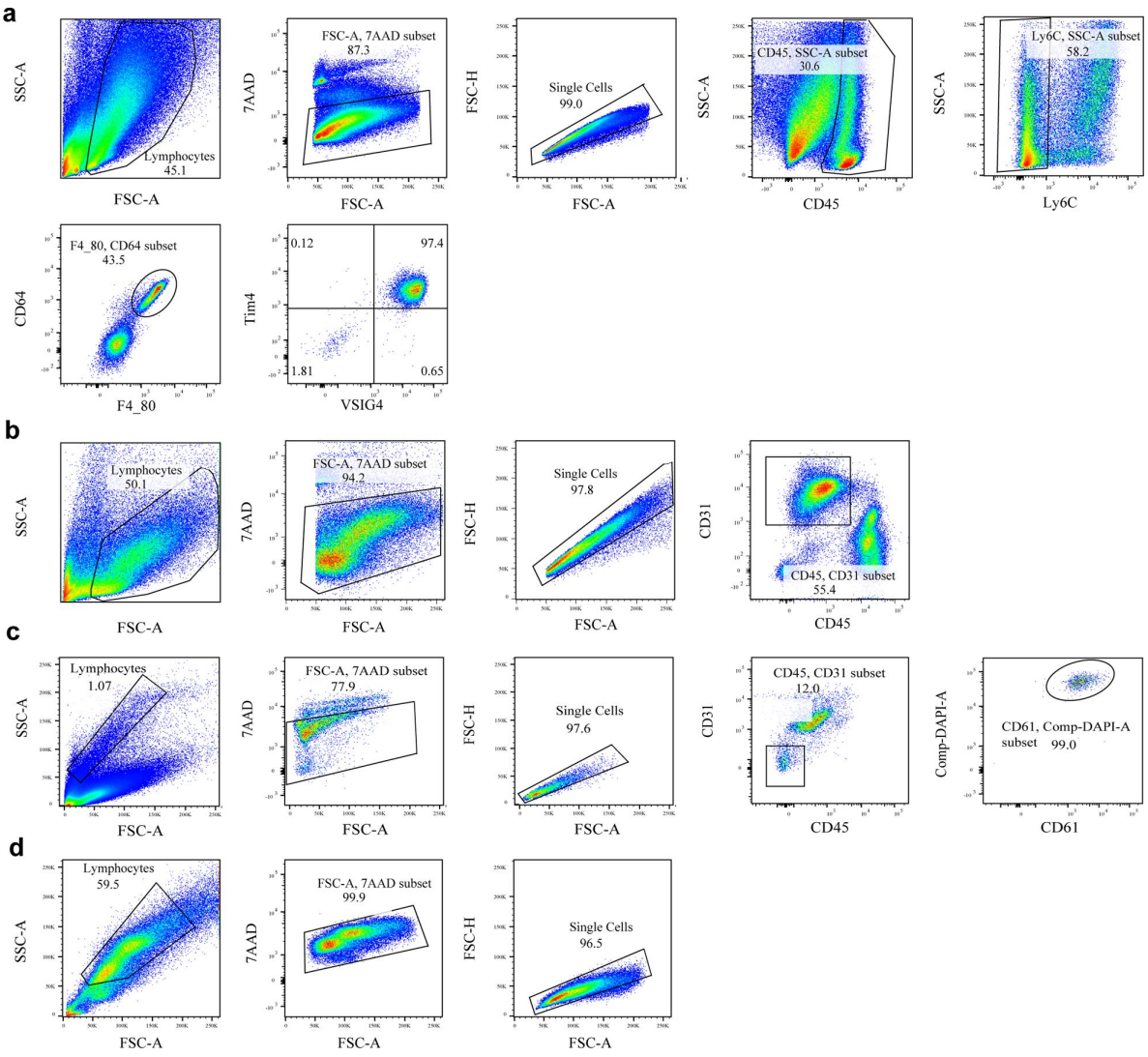

Supplementary Figure 4.

Gating strategies.

(a-d) Gating strategies for KC (a), ECs (b), HSCs (c), and HCs (d) in the liver.

TFs only downregulated in liver macrophages from BMP9/10-HSC KO mice	TFs only downregulated in liver macrophages from Smad4fl/fl Vav1-Cre mice	TFs downregulated in liver macrophages from both BMP9/10-HSC KO mice and Smad4fl/fl Vav1-Cre mice
Cebpe	5730507C01Rik	Creb3l3
Creb3l2	Ahrr	Dmrt2
Epas1	Ascl2	En2
Erg	Batf3	Erf
Esrrb	Dnajc2	Hey1
Foxa3	Gm13212	Id1
Gata4	Jdp2	Id2
Gtf2ird1	Mta3	Id3
Hic1	Pax5	Irf7
Hnf4a	Pou3f1	Nr1h3
Hoxa1	Satb1	Smad7
Hoxa4	Smad4	Smad9
Hoxb5	Zfp941	Thrb
Meis2		Tlx1
Nr1i3		Zbtb18
Ppara		Zbtb4
Purg		Zfp446
Rxra		Zfp532
Six5		Zfp811
Smad6		
Spib		
Tbx3		
Tcf7l1		
Tcf7l2		
Tfec		
Tshz3		
Zfp239		
Zfp507		
Zfp951		

Supplementary table 1.

Transcription factors (TFs) downregulated in liver macrophages from BMP9/10-HSC KO mice and Smad4fl/fl Vav1-Cre mice

Gene	Forward primer	Reverse primer
mouse *Pol2*	CTGGTCCTTCGAATCCGCATC	GCTCGATACCCTGCAGGGTCA
mouse *Bmp9*	CTGGAAGGAAGCATGGTCGT	CCATCCTTCGTCCCGAATGT
mouse *Bmp10*	AACGCCAAGGGGAACTACTG	TTCATACCCAGGAGGAGCGA

Supplementary Table 2.

Primers used for real-time PCR.

4. Young RA (2011) **Control of the embryonic stem cell state** *Cell* **144**:940–954

5. Pancheva A, Wheadon H, Rogers S, Otto TD (2022) **Using topic modeling to detect cellular crosstalk in scRNA-seq** *PLoS Comput Biol* **18**

6. Armingol E, Officer A, Harismendy O, Lewis NE (2021) **Deciphering cell-cell interactions and communication from gene expression** *Nat Rev Genet* **22**:71–88

7. Monga SP (2014) **Role and regulation of beta-catenin signaling during physiological liver growth** *Gene Expr* **16**:51–62

8. Ding C, Li Y, Guo F, Jiang Y, Ying W, Li D, Yang D, et al. (2016) **A Cell-type-resolved Liver Proteome** *Mol Cell Proteomics* **15**:3190–3202

9. Azimifar SB, Nagaraj N, Cox J, Mann M (2014) **Cell-type-resolved quantitative proteomics of murine liver** *Cell Metab* **20**:1076–1087

10. Planas-Paz L, Orsini V, Boulter L, Calabrese D, Pikiolek M, Nigsch F, Xie Y, et al. (2016) **The RSPO-LGR4/5-ZNRF3/RNF43 module controls liver zonation and size** *Nat Cell Biol* **18**:467–479

11. Yang J, Mowry LE, Nejak-Bowen KN, Okabe H, Diegel CR, Lang RA, Williams BO, et al. (2014) **beta-catenin signaling in murine liver zonation and regeneration: a Wnt-Wnt situation!** *Hepatology* **60**:964–976

12. Canali S, Zumbrennen-Bullough KB, Core AB, Wang CY, Nairz M, Bouley R, Swirski FK, et al. (2017) **Endothelial cells produce bone morphogenetic protein 6 required for iron homeostasis in mice** *Blood* **129**:405–414

13. Koch PS, Olsavszky V, Ulbrich F, Sticht C, Demory A, Leibing T, Henzler T, et al. (2017) **Angiocrine Bmp2 signaling in murine liver controls normal iron homeostasis** *Blood* **129**:415–419

14. Efremova M, Vento-Tormo R, Park JE, Teichmann SA, James KR (2020) **Immunology in the Era of Single-Cell Technologies** *Annu Rev Immunol* **38**:727–757

15. Bonnardel J, T'Jonck W, Gaublomme D, Browaeys R, Scott CL, Martens L, Vanneste B, et al. (2019) **Stellate Cells, Hepatocytes, and Endothelial Cells Imprint the Kupffer Cell Identity on Monocytes Colonizing the Liver Macrophage Niche** *Immunity* **51**:638–654

16. Tan Z, Sun H, Xue T, Gan C, Liu H, Xie Y, Yao Y, et al. (2021) **Liver Fibrosis: Therapeutic Targets and Advances in Drug Therapy** *Front Cell Dev Biol* **9**

17. Miyazono K, Kamiya Y, Morikawa M (2010) **Bone morphogenetic protein receptors and signal transduction** *J Biochem* **147**:35–51

18. Schmid CD, Olsavszky V, Reinhart M, Weyer V, Trogisch FA, Sticht C, Winkler M, et al. (2023) **ALK1 controls hepatic vessel formation, angiodiversity, and angiocrine functions in hereditary hemorrhagic telangiectasia of the liver** *Hepatology* **77**:1211–1227

19. Zhao D, Yang F, Wang Y, Li S, Li Y, Hou F, Yang W, et al. (2022) **ALK1 signaling is required for the homeostasis of Kupffer cells and prevention of bacterial infection** *J Clin Invest* **132**

20. Guilliams M, Bonnardel J, Haest B, Vanderborght B, Wagner C, Remmerie A, Bujko A, et al. (2022) **Spatial proteogenomics reveals distinct and evolutionarily conserved hepatic macrophage niches** *Cell* **185**:379–396

21. Bidart M, Ricard N, Levet S, Samson M, Mallet C, David L, Subileau M, et al. (2012) **BMP9 is produced by hepatocytes and circulates mainly in an active mature form complexed to its prodomain** *Cell Mol Life Sci* **69**:313–324

22. Breitkopf-Heinlein K, Meyer C, Konig C, Gaitantzi H, Addante A, Thomas M, Wiercinska E, et al. (2017) **BMP-9 interferes with liver regeneration and promotes liver fibrosis** *Gut* **66**:939–954

23. Lee Y, Leslie J, Yang Y, Ding L (2021) **Hepatic stellate and endothelial cells maintain hematopoietic stem cells in the developing liver** *J Exp Med* **218**

24. Mederacke I, Hsu CC, Troeger JS, Huebener P, Mu X, Dapito DH, Pradere JP, et al. (2013) **Fate tracing reveals hepatic stellate cells as dominant contributors to liver fibrosis independent of its aetiology** *Nat Commun* **4**

25. Sakai M, Troutman TD, Seidman JS, Ouyang Z, Spann NJ, Abe Y, Ego KM, et al. (2019) **Liver-Derived Signals Sequentially Reprogram Myeloid Enhancers to Initiate and Maintain Kupffer Cell Identity** *Immunity* **51**:655–670

26. Herrera B, Dooley S, Breitkopf-Heinlein K (2014) **Potential roles of bone morphogenetic protein (BMP)-9 in human liver diseases** *Int J Mol Sci* **15**:5199–5220

27. Janbandhu VC, Moik D, Fassler R (2014) **Cre recombinase induces DNA damage and tetraploidy in the absence of loxP sites** *Cell Cycle* **13**:462–470

28. Scott CL, Zheng F, De Baetselier P, Martens L, Saeys Y, De Prijck S, Lippens S, et al. (2016) **Bone marrow-derived monocytes give rise to self-renewing and fully differentiated Kupffer cells** *Nat Commun* **7**

29. Tran S, Baba I, Poupel L, Dussaud S, Moreau M, Gelineau A, Marcelin G, et al. (2020) **Impaired Kupffer Cell Self-Renewal Alters the Liver Response to Lipid Overload during Non-alcoholic Steatohepatitis** *Immunity* **53**:627–640

30. Philpott J, Kazimierczyk S, Korgaonkar P, Bordt E, Zois J, Vasudevan C, Meng D, et al. (2022) **RXRalpha Regulates the Development of Resident Tissue Macrophages** *Immunohorizons* **6**:366–372

31. Geraud C, Koch PS, Zierow J, Klapproth K, Busch K, Olsavszky V, Leibing T, et al. (2017) **GATA4-dependent organ-specific endothelial differentiation controls liver development and embryonic hematopoiesis** *J Clin Invest* **127**:1099–1114

32. Gomez-Salinero JM, Izzo F, Lin Y, Houghton S, Itkin T, Geng F, Bram Y, et al. (2022) **Specification of fetal liver endothelial progenitors to functional zonated adult sinusoids requires c-Maf induction** *Cell Stem Cell* **29**:593–609

33. Desroches-Castan A, Tillet E, Ricard N, Ouarne M, Mallet C, Belmudes L, Coute Y, et al. (2019) **Bone Morphogenetic Protein 9 Is a Paracrine Factor Controlling Liver Sinusoidal Endothelial Cell Fenestration and Protecting Against Hepatic Fibrosis** *Hepatology* **70**:1392–1408

34. Winkler M, Staniczek T, Kurschner SW, Schmid CD, Schonhaber H, Cordero J, Kessler L, et al. (2021) **Endothelial GATA4 controls liver fibrosis and regeneration by preventing a pathogenic switch in angiocrine signaling** *J Hepatol* **74**:380–393

35. Ramachandran P, Dobie R, Wilson-Kanamori JR, Dora EF, Henderson BEP, Luu NT, Portman JR, et al. (2019) **Resolving the fibrotic niche of human liver cirrhosis at single-cell level** *Nature* **575**:512–518

36. Aizarani N, Saviano A, Sagar Mailly L, Durand S, Herman JS, Pessaux P, et al. (2019) **A human liver cell atlas reveals heterogeneity and epithelial progenitors** *Nature* **572**:199–204

37. MacParland SA, Liu JC, Ma XZ, Innes BT, Bartczak AM, Gage BK, Manuel J, et al. (2018) **Single cell RNA sequencing of human liver reveals distinct intrahepatic macrophage populations** *Nat Commun* **9**

38. Lu Y, Yang A, Quan C, Pan Y, Zhang H, Li Y, Gao C, et al. (2022) **A single-cell atlas of the multicellular ecosystem of primary and metastatic hepatocellular carcinoma** *Nat Commun* **13**

39. Ma W, Zhao D, He F, Tang L (2019) **The Role of Kupffer Cells as Mediators of Adipose Tissue Lipolysis** *J Immunol* **203**:2689–2700

Article and author information

Dianyuan Zhao

State Key Laboratory of Medical Proteomics, Beijing Proteome Research Center, National Center for Protein Sciences (Beijing), Beijing Institute of Lifeomics, Beijing, 102206, P.R. China

Ziwei Huang

State Key Laboratory of Medical Proteomics, Beijing Proteome Research Center, National Center for Protein Sciences (Beijing), Beijing Institute of Lifeomics, Beijing, 102206, P.R. China, Department of Immunology, School of Basic Medical Sciences, Anhui Medical University, Hefei, Anhui Province, 230032, P.R. China

Xiaoyu Li

State Key Laboratory of Medical Proteomics, Beijing Proteome Research Center, National Center for Protein Sciences (Beijing), Beijing Institute of Lifeomics, Beijing, 102206, P.R. China, Department of Immunology, School of Basic Medical Sciences, Anhui Medical University, Hefei, Anhui Province, 230032, P.R. China

Huan Wang

State Key Laboratory of Medical Proteomics, Beijing Proteome Research Center, National Center for Protein Sciences (Beijing), Beijing Institute of Lifeomics, Beijing, 102206, P.R. China

Qingwei Hou

State Key Laboratory of Medical Proteomics, Beijing Proteome Research Center, National Center for Protein Sciences (Beijing), Beijing Institute of Lifeomics, Beijing, 102206, P.R. China, School of Basic Medicine, Qingdao University, Qingdao, Shandong Province, 266071, P.R. China

Yuyao Wang
State Key Laboratory of Medical Proteomics, Beijing Proteome Research Center, National Center for Protein Sciences (Beijing), Beijing Institute of Lifeomics, Beijing, 102206, P.R. China, School of Basic Medicine, Qingdao University, Qingdao, Shandong Province, 266071, P.R. China

Fang Yan
State Key Laboratory of Medical Proteomics, Beijing Proteome Research Center, National Center for Protein Sciences (Beijing), Beijing Institute of Lifeomics, Beijing, 102206, P.R. China

Wenting Yang
State Key Laboratory of Medical Proteomics, Beijing Proteome Research Center, National Center for Protein Sciences (Beijing), Beijing Institute of Lifeomics, Beijing, 102206, P.R. China

Di Liu
State Key Laboratory of Medical Proteomics, Beijing Proteome Research Center, National Center for Protein Sciences (Beijing), Beijing Institute of Lifeomics, Beijing, 102206, P.R. China

Shaoqiong Yi
State Key Laboratory of Medical Proteomics, Beijing Proteome Research Center, National Center for Protein Sciences (Beijing), Beijing Institute of Lifeomics, Beijing, 102206, P.R. China

Chunguang Han
State Key Laboratory of Medical Proteomics, Beijing Proteome Research Center, National Center for Protein Sciences (Beijing), Beijing Institute of Lifeomics, Beijing, 102206, P.R. China

Yanan Hao
State Key Laboratory of Medical Proteomics, Beijing Proteome Research Center, National Center for Protein Sciences (Beijing), Beijing Institute of Lifeomics, Beijing, 102206, P.R. China

Li Tang
State Key Laboratory of Medical Proteomics, Beijing Proteome Research Center, National Center for Protein Sciences (Beijing), Beijing Institute of Lifeomics, Beijing, 102206, P.R. China, Department of Immunology, School of Basic Medical Sciences, Anhui Medical University, Hefei, Anhui Province, 230032, P.R. China, School of Basic Medicine, Qingdao University, Qingdao, Shandong Province, 266071, P.R. China
For correspondence: tangli@ncpsb.org.cn
ORCID iD: 0000-0002-6514-9266

Copyright

Editors

Reviewing Editor
Paschalis Kratsios
University of Chicago, Chicago, United States of America

Senior Editor
Pramod Mistry
Yale University, New Haven, United States of America

Reviewer #1 (Public Review):

Summary:

The aim of the present work is to evaluate the role of BMP9 and BMP10 in liver by depleting Bmp9 and Bmp10 from the main liver cell types (endothelial cells (EC), hepatic stellate cells (HSC), Kupffer cells (KC) and hepatocytes (H)) using cell-specific cre recombinases. They show that HSCs are the main source of BMP9 and BMP10 in the liver. Using transgenic ALK1 reporter mice, they show that ALK1, the high affinity type 1 receptor for BMP9 and BMP10, is expressed on KC and EC. They have also performed bulk RNAseq analyses on whole liver, and cell-sorted EC and KC, and showed that loss of Bmp9 and Bmp10 decreased KC signature and that KC are replaced by monocyte-derived macrophages. EC derived from these Bmp9fl/flBmp10fl/flLratCre mice also lost their identity and transdifferentiated into continuous ECs. Liver iron metabolism and metabolic zonation were also affected in these mice. In conclusion, this work supports that BMP9 and BMP10 produced by HSC play a central role in mediating liver cell-cell crosstalk and liver homeostasis.

Strengths:

This work further supports the role of BMP9 and BMP10 in liver homeostasis. Using a specific HSC-Cre recombinase, the authors show for the first time that it is the BMP9 and BMP10 produced by HSC that play a central role in mediating liver cell-cell crosstalk to maintain a healthy liver. Although the overall message of the key role of BMP9 in liver homeostasis has been described by several groups, the role of hepatic BMP10 has not been studied before. Thus, one of the novelties of this work is to have used liver cell specific Cre recombinase to delete hepatic Bmp9 and Bmp10. The second novelty is the demonstration of the role of BMP9 and BMP10 in KC Differentiation/homeostasis which has already been slightly addressed by this group by knocking out ALK1, the high affinity receptor of BMP9 and BMP10 (Zhao et al. JCI, 2022).

Weaknesses:

This work remains rather descriptive and the molecular mechanisms are barely touched upon and could have been more explored.
Some references should be added; In particular, a work that has already demonstrated, using a different approach (in situ hybridization RNAscope), that in the liver BMP9 and BMP10 are expressed by HSC (Tillet et al., J Biol Chem 2018). Another publication (Bouvard et al., Cardiovasc Res, 2021) has previously showed that deletion of Bmp9 and Bmp10 leads to liver fibrosis and could have thus been cited. There is also a reference that is not correctly cited. Ref 26 (Herrera et al., 2014) does not say that "BMP10 is mostly expressed in the heart, followed by the liver" or that "BMP9 and BMP10 also bind to ALK2" as cited in the manuscript.
The gating strategies for cell sorting which is used for bulk RNAseq and FACS analyses should be better described in order to better follow the manuscript. This point is particularly important for KC gating as the authors show that Tim4 is very strongly decreased in Bmp9fl/flBmp10fl/flLratCre (Fig 2c), yet, it seems that this marker is used for gating macrophages (Suppl fig4). Same question with F4/80 which is strongly decreased in Bmp9fl/flBmp10fl/flLratCre (Fig 2d) and also used for gating. It is important to show the gating strategy for both Control and Bmp9fl/flBmp10fl/flLratCre mice.
The authors should explain how they selected the genes shown on each heatmaps and add references that can justify the choice of the genes.

Quantifications of Immunostaining and FACS data should be added as well as statistical analyses.

https://doi.org/10.7554/eLife.95811.1.sa1

Reviewer #2 (Public Review):

Summary:

The authors characterized the contribution of BMP9/BMp10 expression/secretion from all different hepatic cell types and analysed their impact on the other cell types. They are able to show that HSC derived BMP9/BMP10 controls Kupffer cell and EC differentiation and functions.

Strengths:

This is the first study to my knowledge to comprehensively analyze the contribution of BMP9/BMP10 expression in such systematic fashion in vivo. This study therefore is a significant contribution to the field and further supports previous studies that have already implied BMP9 and BMP10 in Kupffer cell and EC functions but did not unravel the intercellular cross talk in such detailed fashion.

Weaknesses:

Several findings such as the impact of BMP9/10 on Kupffer cells and EC were already known. So these findings are not innovative, however I still believe that the elucidation of the cellular crosstalk makes this publication highly interesting to a broad scientific community.

Overall the authors achieved their aims and the results are well supporting the conclusions and discussion.

https://doi.org/10.7554/eLife.95811.1.sa0

Author response:

> ***Public Reviews:***
>
> ***Reviewer #1 (Public Review):***
>
> *Summary:*
>
> *The aim of the present work is to evaluate the role of BMP9 and BMP10 in liver by depleting Bmp9 and Bmp10 from the main liver cell types (endothelial cells (EC), hepatic stellate cells (HSC), Kupffer cells (KC) and hepatocytes (H)) using cell-specific cre recombinases. They show that HSCs are the main source of BMP9 and BMP10 in the liver. Using transgenic ALK1 reporter mice, they show that ALK1, the high affinity type 1 receptor for BMP9 and BMP10, is expressed on KC and EC. They have also performed bulk RNAseq analyses on whole liver, and cell-sorted EC and KC, and showed that loss of Bmp9 and Bmp10 decreased KC signature and that KC are replaced by monocyte-derived macrophages. EC derived from these Bmp9fl/flBmp10fl/flLratCre mice also lost their identity and transdifferentiated into continuous ECs. Liver iron metabolism and metabolic zonation were also affected in these mice. In conclusion, this work supports that BMP9 and BMP10 produced by HSC play a central role in mediating liver cell-cell crosstalk and liver homeostasis.*

We appreciate the comprehensive summary of reviewer 1.

> *Strengths:*
>
> *This work further supports the role of BMP9 and BMP10 in liver homeostasis. Using a specific HSC-Cre recombinase, the authors show for the first time that it is the BMP9 and BMP10 produced by HSC that play a central role in mediating liver cell-cell crosstalk to maintain a healthy liver. Although the overall message of the key role of BMP9 in liver homeostasis has been described by several groups, the role of hepatic BMP10 has not been studied before. Thus, one of the novelties of this work is to have used liver cell specific Cre recombinase to delete hepatic Bmp9 and Bmp10. The second novelty is the demonstration of the role of BMP9 and BMP10 in KC Differentiation/homeostasis which has already been slightly addressed by this group by knocking out ALK1, the high affinity receptor of BMP9 and BMP10 (Zhao et al. JCI, 2022).*

We appreciate the positive comment of reviewer 1.

> *Weaknesses:*
>
> *This work remains rather descriptive and the molecular mechanisms are barely touched upon and could have been more explored. Some references should be added; In particular, a work that has already demonstrated, using a different approach (in situ hybridization RNAscope), that in the liver BMP9 and BMP10 are expressed by HSC (Tillet et al., J Biol Chem 2018). Another publication (Bouvard et al., Cardiovasc Res, 2021) has previously showed that deletion of Bmp9 and Bmp10 leads to liver fibrosis and could have thus been cited. There is also a reference that is not correctly cited. Ref 26 (Herrera et al., 2014) does not say that "BMP10 is mostly expressed in the heart, followed by the liver" or that "BMP9 and BMP10 also bind to ALK2" as cited in the manuscript.*

We agree with the comment of reviewer 1 that the molecular mechanisms were barely investigated in our work. Indeed, it has been reported that BMP9/10 induce the expression of ID1/3 in KCs and GATA4 and Maf in liver ECs in vitro culture system. These master regulators play an important role in the differentiation of the two cell types. Thus, we think that the reduced expression of these master regulators can explain the phenotype in KCs and ECs observed in Bmp9fl/flBmp10fl/flLratCre mice. In addition, according to the reviewer's suggestion, these references will be added or corrected in our revised manuscript.

> *The gating strategies for cell sorting which is used for bulk RNAseq and FACS analyses should be better described in order to better follow the manuscript. This point is particularly important for KC gating as the authors show that Tim4 is very strongly decreased in Bmp9fl/flBmp10fl/flLratCre (Fig 2c), yet, it seems that this marker is used for gating macrophages (Suppl fig4). Same question with F4/80 which is strongly decreased in Bmp9fl/flBmp10fl/flLratCre (Fig 2d) and also used for gating. It is important to show the gating strategy for both Control and Bmp9fl/flBmp10fl/flLratCre mice.*
>
> *The authors should explain how they selected the genes shown on each heatmaps and add references that can justify the choice of the genes.*

Thank you for your suggestion. In our study, we used CD45+ Ly6C- F4/80+ CD64+ cells to define liver macrophages. We will delete Tim4 FACS plot from Suppl fig4 to avoid the misunderstanding. Although F4/80 positive cells were reduced in the livers of Bmp9fl/flBmp10fl/flLratCre mice, double staining by anti-F4/80 and anti-CD64 fluorescence antibodies can still clearly distinguish liver macrophages based on above gating strategy.

Gating strategy for both control and Bmp9fl/flBmp10fl/flLratCre mice will be presented in our revised manuscript.

> *Quantifications of Immunostaining and FACS data should be added as well as statistical analyses.*

Quantitative data will be added in our revised manuscript.

> ***Reviewer #2 (Public Review):***
>
> *Summary:*
>
> *The authors characterized the contribution of BMP9/BMP10 expression/secretion from all different hepatic cell types and analysed their impact on the other cell types. They are able to show that HSC derived BMP9/BMP10 controls Kupffer cell and EC differentiation and functions.*

We appreciate the comprehensive summary of reviewer 2.

> *Strengths:*
>
> *This is the first study to my knowledge to comprehensively analyze the contribution of BMP9/BMP10 expression in such systematic fashion in vivo. This study therefore is a significant contribution to the field and further supports previous studies that have already implied BMP9 and BMP10 in Kupffer cell and EC functions but did not unravel the intercellular cross talk in such detailed fashion.*

We appreciate the positive comment of reviewer 2.

> *Weaknesses:*
>
> *Several findings such as the impact of BMP9/10 on Kupffer cells and EC were already known. So these findings are not innovative, however I still believe that the elucidation of the cellular crosstalk makes this publication highly interesting to a broad scientific community.*
>
> *Overall the authors achieved their aims and the results are well supporting the conclusions and discussion.*

We appreciate the positive comment of reviewer 2. We agree with the comment of reviewer 2 that although some findings in our paper are somehow expected, the detailed investigation of the crosstalk between different liver cell types is still needed and beneficial to this field.